

Numerical studies of laser-induced energy deposition for supersonic flow control

Ramnath Kandala, Graham V. Candler*

University of Minnesota, Department of Aerospace Engineering and Mechanics, Minneapolis MN 55455, USA

Abstract

This paper deals with the computational study of localized laser energy deposition in three-dimensional supersonic flows. A model for Nd:YAG laser energy deposition in air has been developed to capture the key physical processes including the energy absorption and the resulting fluid dynamics. Energy deposition was found to be effective in reducing the peak surface pressure in flows with Edney Type IV shock–shock interaction, while in flows with intersecting oblique shocks in dual-solution domain, it led to a transition from Mach reflection to regular reflection for certain flow configurations.

Keywords: Supersonic flow control; Laser energy deposition; CFD

1. Introduction

When a powerful laser is focused into air or onto a target, an intense spark or plasma is formed. Energy deposition increases the gas temperature in the plasma region and produces a pressure wave, which can be used to modify the local flow to achieve the desired effect. For example, experiments [1] have shown that the detrimental effects of a shock–shock interaction (which can occur on an air vehicle during maneuver) can be mitigated using localized energy deposition. In this work, we use numerical simulations to study the effects of Nd:YAG laser energy deposition in supersonic flows with shock interactions, using computational simulations. The simulation of the energy deposition process was performed using a model that we have developed [2]. Two kinds of supersonic flows are considered here—flows with Edney Type IV shock–shock interaction and flows with intersecting oblique shocks.

2. Mathematical formulation

2.1. Plasma formation model

The series of steps involved in the laser energy

deposition into a gas are illustrated in Fig. 1. The numerical model was designed to capture key features of this process. A small number of seed electrons is used to initiate the electron cascade by absorbing the laser light at the beginning of the simulation. The inverse bremsstrahlung absorption is modeled using the absorptivity coefficient κ_a , while the expansion of plasma region is accounted for by introducing the concept of reflectivity, characterized by coefficient κ_r . As the plasma density increases, the laser light is scattered due to reflection. Some of this light is re-absorbed by the adjacent cooler gas to trigger cascade ionization in those regions.

Due to laser absorption, the intensity of the laser beam, I , varies in the direction of laser propagation, x :

$$\frac{dI}{dx} = -\kappa_a I \quad (1)$$

By integrating the above equation and assuming a constant $\kappa_{a,i,j}$ over a grid cell, $q_{abs,i,j}$, the average absorption rate inside a cell of width $\Delta x_{i,j}$, along the direction of light propagation (i -direction), as a function of the intensity is:

$$q_{abs,i,j} = I_{i,j} \frac{1 - \exp(-\kappa_{a,i,j} \Delta x_{i,j})}{\Delta x_{i,j}} \quad (2)$$

where $I_{i,j} = (I - \kappa_{r,i,j}) I_{s,i,j} + \alpha_{i,j} \kappa_{r,i+1,j} I_{s,i+1,j}$
 $I_{s,i,j}$ is the intensity of the incident light for the cell (i, j).

* Corresponding author. Tel.: +1 612 625 2364; Fax: +1 612 626 1558; E-mail: candler@aem.umn.edu

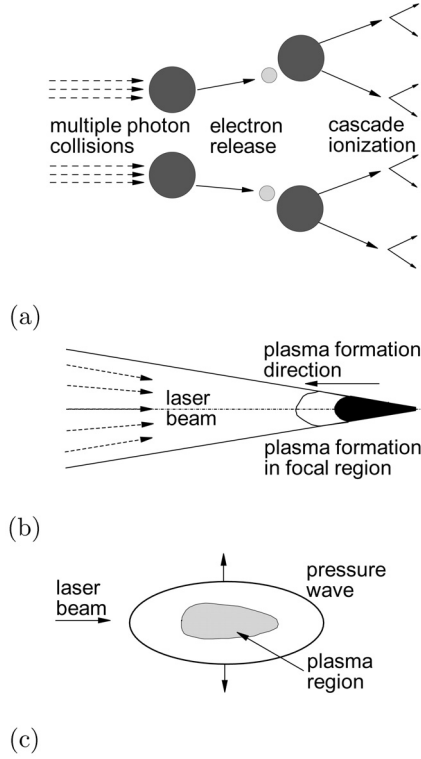


Fig. 1. Schematic, showing the sequence of steps leading to laser energy deposition in air.

α_{ij} is the fraction of the energy from the cell $(i + 1, j)$ that reaches the cell (i, j) . κ_a is given by:

$$\kappa_a = \frac{Q}{T} n_e (1 - \exp(-hc/\lambda k T_e)) \quad (3)$$

where Q is defined as the characteristic cross-section of absorption. The plasma is transparent to the laser light in the initial stages, but it becomes opaque gradually. Thus, the reflectivity coefficient, κ_r , depends on the fraction of ionization, Z , and varies between 0 and 1.

$$\kappa_r = A (\log(Z) + B) \quad (4)$$

The unknowns in the above analysis are Q , the characteristic area of cross-section, and A and B , the constants for the reflectivity coefficient. We determine their values by matching the properties of the plasma and the resulting pressure wave to experiments (Kandala et al. [2]).

2.2. Chemical kinetics and conservation equations

In this flow we assume that eleven species may be present in appreciable quantities: N_2 , O_2 , NO , N , O ,

N_2^+ , O_2^+ , NO^+ , N^+ , O^+ , and electrons. A chemical kinetics model for two-temperature air (translational-rotational and electron temperatures) developed by Laux et al. [3] is used.

We solve mass conservation equations for each of the eleven species, momentum conservation equations for the axial and radial momenta, and energy conservation equations for total, vibrational, and electron energies.

$$\frac{\partial \rho_s}{\partial t} + \nabla \cdot (\rho_s \mathbf{u}) = -\nabla \cdot (\rho_s \mathbf{v}_s) + w_s \quad (5)$$

$$\frac{\partial}{\partial t} (\rho \mathbf{u}) + \nabla \cdot (\rho \mathbf{u} \otimes \mathbf{u}) = -\nabla p - \nabla \cdot \tilde{\tau} \quad (6)$$

$$\begin{aligned} \frac{\partial E}{\partial t} + \nabla \cdot ((E + p) \mathbf{u}) = & -\nabla \cdot (\mathbf{q} + \mathbf{q}_v + \mathbf{q}_e) - \nabla \cdot (\mathbf{u} \cdot \tilde{\tau}) - \\ & \nabla \cdot \sum_{s=1}^n (\mathbf{v}_s \rho_s h_s) + Q_r \end{aligned} \quad (7)$$

$$\begin{aligned} \frac{\partial E_v}{\partial t} + \nabla \cdot (E_v \mathbf{u}) = & -\nabla \cdot \mathbf{q}_v - \nabla \cdot \sum_{s=1}^n \mathbf{v}_s E_{v,s} + Q_{T-v} + \\ & Q_{e-v} + \sum_{s=1}^n w_s e_{v,s} \end{aligned} \quad (8)$$

$$\begin{aligned} \frac{\partial E_e}{\partial t} + \nabla \cdot ((E_e + p_e) (\mathbf{u} + \mathbf{v}_e)) = & -\nabla \cdot \mathbf{q}_e - Q_{h-e} - \\ & Q_{v-e} + Q_r + w_e e_e \end{aligned} \quad (9)$$

The radiative energy addition and loss is represented in the electron energy conservation equation by Q_r . In the present case Q_r is equal to q_{abs} . See [2] for more details.

3. Numerical aspects

The initiation of electron cascade is characterized by time scales of one nanosecond or less, while the pressure wave expansion around the plasma region occurs at a time scale of about $10 \mu s$. To handle this disparity, we linearize those source terms that are relatively fast. This results in a semi-implicit method which substantially increases the stable time step.

The fast terms include some species production terms, the internal energy relaxation, and the electron heating source terms. The conservation equations are then written in axisymmetric coordinates as:

$$\frac{\partial U}{\partial t} + \frac{\partial F}{\partial x} + \frac{1}{r} \frac{\partial rG}{\partial r} = W_{fast} + W_{slow} \quad (10)$$

We linearize W_{fast} in time:

$$W_{fast}^{n+1} = W_{fast}^n + C_{fast}^n \delta U^n + O(\Delta t^2) \quad (11)$$

where C_{fast} is the Jacobian of W_{fast} with respect to U ,

and $\delta U^n = U^{n+1} - U^n$. Then, the solution is integrated in time using:

$$\delta U^{n+1} = (I - \Delta t C_{fast}^n)^{-1} \Delta t \left((W_{fast}^n + W_{slow}^n) - \left(\frac{\partial F^n}{\partial x} + \frac{1}{r} \frac{\partial r G^n}{\partial r} \right) \right) \quad (12)$$

4. Energy deposition in supersonic flows

Three-dimensional CFD simulations were performed to study the effect of energy deposition in three-dimensional flows. Energy from a laser discharge was deposited upstream of a sphere in a steady supersonic flow. This was achieved by focusing a laser beam upstream of the flow, in a direction perpendicular to the flow field. The flow conditions were chosen to simulate the experiments presented in Adelgren et al. [1].

In the simulations, the plasma formation and its evolution into a pressure wave was simulated until $0.5 \mu s$

on an axisymmetric domain, and then superimposed onto the three-dimensional steady supersonic flow. The three-dimensional flow was simulated using the data parallel line relaxation (DPLR) method, Wright et al. [4].

4.1. Edney Type IV shock–shock interaction

Edney Type IV shock–shock interactions occur in a supersonic flow when an oblique shock impinges onto the bow shock in front of the leading edge of the sphere. This leads to high localized heat transfer rate and surface pressure on the sphere, in the region just above the oblique shock. The pressure contours of the energy spot interaction with the flow are shown in Fig. 2. As the energy spot moves downstream, the high temperature region changes the local Mach number and deforms the oblique shock ($t = 20 \mu s$ in Fig. 2).

The high temperature region in the energy spot causes the shock to bulge, resulting in a decrease in the surface pressure. It was found that the peak pressure decreases by up to 70% during this period. No significant decrease

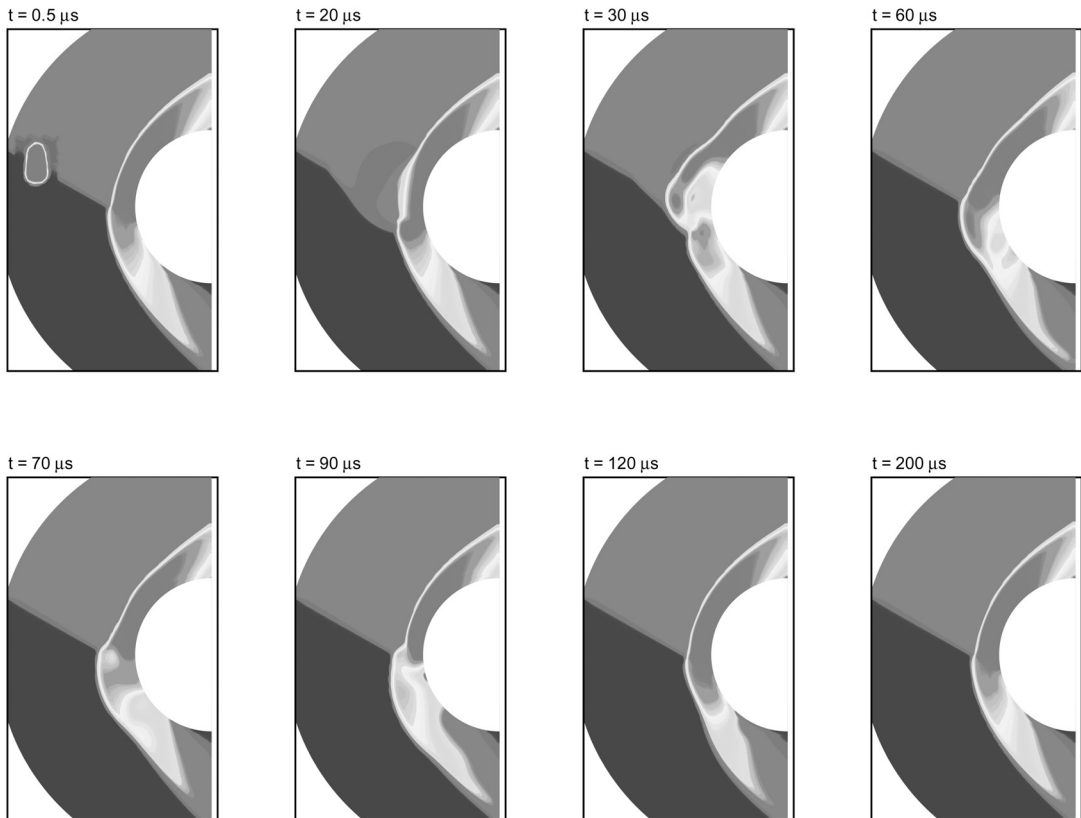


Fig. 2. Pressure contours for energy deposition in a flow with Edney Type IV shock–shock interaction (Mach 3.45 flow with 15° flow turn angle) at various times.

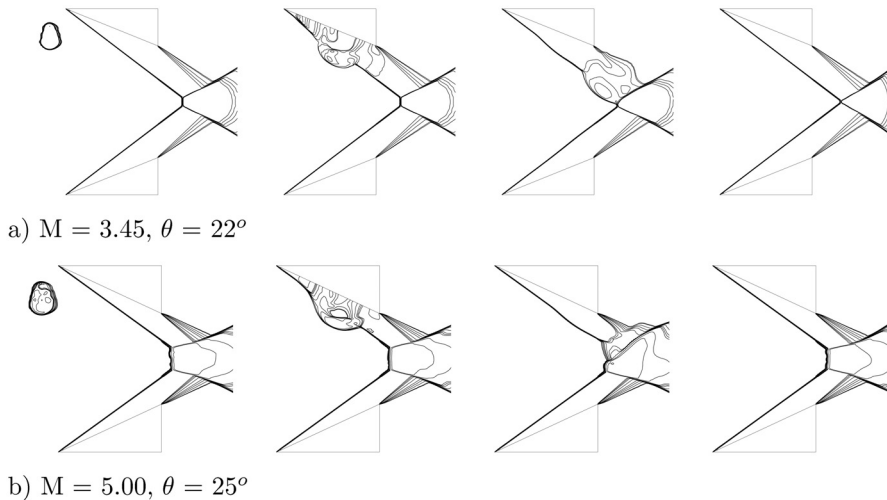


Fig. 3. Pressure contours, on the x - y plane of symmetry, showing the interaction of the energy spot with the flow at different times (θ is the flow deflection angle).

in the heat transfer rate was observed in these simulations.

4.2. Crossing shock waves

When two symmetric oblique shocks intersect, the shock–shock interaction can lead to either a regular reflection (RR) or a Mach reflection (MR), depending on the shock angle and the freestream Mach number. However, within a certain range of shock angles, and above a certain Mach number, both types of reflection are theoretically possible, i.e. a dual solution domain (DSD) exists. In our simulations, MR was created using supersonic flow past two finite span symmetric wedges, in the DSD. Then the laser energy was deposited upstream of this flow. Our simulations were guided by experiments and numerical simulations conducted at Rutgers University (Adelgren et al. [1] and Yan et al. [5]).

The computations were performed using a three-dimensional multi-block grid (5 million grid points) for different cases, while varying the Mach number, Mach angle, initial position of the energy spot, and the number of energy spots input. Figure 3 illustrates two cases of simulations: (a) $M = 3.45$, wedge angle, $\theta = 22^\circ$; (b) $M = 5.0$, $\theta = 25^\circ$. The figures show that, due to the perturbation of the shock structures, MR \rightarrow RR transition occurs in the $M = 3.45$ case, while the MR remains unaltered in the $M = 5.0$ case. The results of various cases showed that the transition is affected by the flow configuration and the initial location of the energy spot.

5. Conclusions

We have performed a computational study of laser energy deposition in three-dimensional supersonic flows as a means of localized flow control. A laser energy deposition model was developed in this work, which captures the energy absorption mechanism by using the concepts of absorption and reflection of laser light. An eleven species finite-rate chemical kinetics model was used to simulate the air breakdown. The simulations showed that the energy spot affects the shock structures in flows with Edney Type IV shock–shock interactions, leading to a decrease in the peak pressure. In flows with intersecting shocks, the energy spot brought about a MR \rightarrow RR transition in dual solution domain, for certain flow configurations.

Acknowledgments

This research is supported by Air Force Office of Scientific Research (AFOSR) under Grant No. F49620–01–1–0368. The views and conclusions contained herein are those of the authors and should not be interpreted as necessarily representing the official policies or endorsements, either expressed or implied, of the AFOSR or the US Government.

References

- [1] Adelgren RG, Yan H, Elliott GS, Knight DD, Beutner T, Zheltovodov AA, Ivanov M, Khotyanovsky D. Localized

- flow control by laser energy deposition applied to Edney IV shock impingement and intersecting shocks. AIAA Paper 2003-0031, January 2003.
- [2] Kandala R, Candler GV. Numerical studies of laser-induced energy deposition for supersonic flow control. AIAA Journal 2004;42(11):2266-2275.
- [3] Laux C, Pierrot L, Gessman R, Kruger CH. Ionization mechanisms of two-temperature plasmas. AIAA Paper 1999-3476, June, 1999.
- [4] Wright MJ, Bose D, Candler GV. A data-parallel line relaxation method for the Navier-Stokes equations. AIAA Journal 1998;36,9:1603-1609.
- [5] Yan H, Adelgren R, Elliott G, Knight D, Beutner T. Effect of energy addition on MR-RR transition. Shock Waves 2003;13:113-121.